SUPPLEMENTARY MATERIALS

Thoracic Spinal Cord Neuroinflammation as a Novel Therapeutic Target in Pulmonary Hypertension

Asif Razee, M.Sc, Somanshu Banerjee PhD, Jason Hong MD, PhD, Shino Magaki, MD, PhD, Greg Fishbein, MD, Olujimi A. Ajijola, MD, PhD, Soban Umar, MD, PhD

Running title: Spinal Cord Neuroinflammation in PH

Materials and Methods

All animal studies were performed in accordance with the National Institutes of Health (NIH) Guide for the Care and Use of Laboratory Animals. Protocols received UCLA animal research committee approval.

Animal Models of Pulmonary Hypertension

Adult male Sprague Dawley rats (250-350g) received either a single subcutaneous injection of pulmonary endothelial toxin Monocrotaline (MCT, 60mg/kg, n=8) and were followed for 30 days or VEGF-receptor antagonist Sugen (SU5416, 20mg/kg, SuHx group, n=8) and kept in hypoxia (10% oxygen) for 3-weeks followed by 2-weeks of normoxia. PBS treated rats served as controls (CTRL, n=8). Serial transthoracic echocardiography was performed to monitor cardiopulmonary hemodynamics and development of PH and RV dysfunction. Direct RV and LV catheterization was performed terminally, and RV hypertrophy index was calculated as the weight ratio of RV/(LV+IVS). Thoracic and lumbar spinal cord tissue were collected.

Intrathecal Minocycline Injection

Intrathecal minocycline injections were performed daily on a group of MCT-treated rats from day 14-28 post MCT injection and were compared with MCT rats treated with daily intrathecal PBS (n=5 per group). Briefly, rats were anesthetized with isoflurane/O2 mixture (3-4%), and body temperature was maintained at 37±1°C using heating pads. MCT-treated rats either received daily intrathecal Minocycline (200μg/kg, Sigma-Aldrich, St. Louis, MO in 30μl PBS)[21,26] or 30μl PBS from day 14-28. Intrathecal injections were administered with a 29-gage needle at L4-5 level to avoid spinal cord injury; successful injections were documented with prominent tail flicks.

Role of TRPV1 Receptors in Bradykinin-induced Cardiopulmonary Sympathetic Afferent Signaling in MCT Rats

To determine whether TRPV1 receptors mediate the bradykinin-induced cardiopulmonary sympathetic afferent transmission in PH, change in heart rate and blood pressure to RV-epicardial and pulmonary vascular application of bradykinin were measured in MCT and control rats (n=5 per group). After tracheostomy and thoracotomy, direct right heart catheterization (Millar SPR-671) was performed terminally to record baseline right ventricular systolic pressure (RVSP) and heart rate for 10 min. Bradykinin (60 μg/mL; Sigma, B3259)[23] was dissolved in 0.1M acetic acid+PBS and applied to the anterior surface of the right ventricle as well as pulmonary vasculature with a pipette. Following bradykinin application, the RVSP and heart rate were recorded continuously for another 5 min.

Diagnosis and Clinical characteristics of PAH Patients and Controls

Thoracic spinal cord (TSC) autopsy samples from 3 control subjects and 3 patients with PAH were obtained from UCLA Department of Pathology. Formal consents were obtained for the use of autopsy tissue for research.

Controls: Control subjects did not have evidence of PH or RV dysfunction.

Control 1: 69 y/o female with history of renal failure.
Control 2: 70 y/o female with history of hip fracture and incarcerated hiatal hernia.
Control 3: 29 y/o male with history of cancer.
PH patients: PH patients had documented diagnosis of PH.
Patient 1: 69 y/o male with group I PH secondary to portopulmonary hypertension (RVSP 43 mmHg; TAPSE 3.2cm).
Patient 2: 68 y/o male with group III PH secondary to COPD and alpha 1 antitrypsin deficiency (RVSP 40 mmHg; TAPSE 2.4cm; PVR 3.6 Woods Unit; reduced RV function).
Patient 3: 68 y/o female with group I PH secondary to connective tissue disease, scleroderma (RVSP 87 mmHg; reduced RV function; RVFAC 20%; TAPSE 1.7cm; RVWT 7mm).

RNA Sequencing Analysis
RNA-Seq was performed on rat TSC tissue. Libraries for RNA-Seq were prepared using SMARTer Stranded Total RNA-Seq Kit v2 - Pico Input Mammalian (Takara Bio). The resulting libraries were sequenced as single-end 50 base pair reads using NextSeq400 (Illumina). Reads were aligned to Rnor 6.0 genome using HISAT2 version 2.1.0 and transcripts were assembled and quantified using StringTie version v1.3.3b. Differential expression analysis was conducted using the R-program DeSeq2 version 1.25.16 correcting for multiple hypothesis testing using the Benjamini Hochberg method. Differentially expressed genes (DEGs) with FDR<0.05 were considered statistically significant. Gene set enrichment analysis was performed using the Bioconductor (release 3.1) fgsea[1] and R (version 3.6.1) software package. Hallmark[2] gene sets were obtained from molecular signature database (MSigDB)[3]. Enriched pathways considered statistically significant were defined by adjusted *p*-value <0.05.

Echocardiography and cardiopulmonary hemodynamic measurements
Transthoracic echocardiograms (VisualSonics Vevo3100, Toronto, Canada) were obtained using a rat specific probe (25 MHZ). Rats were anesthetized *via* inhaled isuflourane at 2-3%. Each rat was placed in supine position, and body temperature was maintained at 37°C. Echocardiograms including B-mode, M-mode and pulsed-wave Doppler images were obtained under isoflurane aesthesia. RV fractional area change (RVFAC, %) was measured from parasternal short-axis view at mid-papillary level. RV internal diameter at end-diastole (RVIDd) was measured using M-mode, parasternal short or long-axis views. LV ejection fraction (LVEF, %) was measured using M-mode echocardiographic images and pulmonary artery acceleration time (PAT) was assessed by pulmonary pulsed-wave doppler echocardiography of PA flow. The probe was placed in a parasternal long-axis position to visualize the PA outflow tract. Pulsed flow doppler imaging was then overlaid to observe the dynamics of blood flow through the PA valve. PAT was determined by calculating time taken from the start of flow to maximal velocity using echocardiogram software.
The right ventricular systolic pressure (RVSP) and left ventricular systolic pressure (LVSP) were measured directly by inserting a catheter (1.4 F Millar SPR-671, ADInstruments) connected to a pressure transducer (Power Lab, ADInstruments) into the RV or LV just before sacrifice. Briefly, for cardiac catheterization, the rats were anesthetized with isoflurane. The animals were placed on a controlled warming pad to

keep the body temperature constant at 37 °C. After a tracheotomy was performed, a cannula was inserted, and the animals were mechanically ventilated. After a midsternal thoracotomy, rats were placed under a stereomicroscope (Zeiss, Hamburg, Germany) and a pressure-conductance catheter (model 1.4 F Millar SPR-671) was introduced via the apex into the RV or LV and positioned towards the pulmonary or aortic valve respectively. The catheter was connected to a signal processor (ADInstruments) and pressures were recorded digitally. After recording the pressures, heart, lung and spinal cord tissues were removed rapidly under deep anesthesia for preservation of protein and RNA integrity.

Gross histologic analysis, tissue preparation and imaging

The right ventricular (RV) wall, the left ventricular (LV) wall, and the interventricular septum (IVS) were dissected. RV, LV, IVS and lungs were weighed. The ratio of the RV to LV plus septal weight [RV/(LV + IVS)] was calculated as the Fulton index of RV hypertrophy. Whole lungs were isolated and inflated manually using a syringe by perfusing 4% paraformaldehyde in 0.1 M Na_2HPO_4 and 23 mM NaHPO4 (pH 7.4) through trachea. Isolated perfused lungs were fixed in 4% paraformaldehyde for 4 h on ice. Spinal cords were fixed in 4% paraformaldehyde (PFA) in 0.1 M Na_2HPO_4 and 23 mM $NaHPO_4$ (pH 7.4) for 4h on ice. Lung and spinal cord tissue was then immersed in ice-cold 20% sucrose in 0.1 M Na_2HPO_4 and 23 mM $NaHPO_4$ (pH 7.4) overnight to cryoprotect the tissue, mounted using OCT, and transversal 4–6µm sections were obtained with a cryostat. Lung tissue sections were stained with Masson's trichrome staining. Images were acquired using a confocal microscope (Nikon).

RNA Extraction and qRT-PCR

Real-time quantitative reverse transcription PCR (qRT-PCR) was performed with total RNA that was extracted from the thoracic and lumbar regions of spinal cord from control, MCT and SuHx rats using Trizol (Invitrogen) according to the manufacturer's instructions. Two micrograms of total RNA were used for the cDNA synthesis using iScript™ cDNA Synthesis Kit (Bio-Rad). Target mRNAs were detected and quantified by a real-time PCR instrument (CFX96 Touch, Bio-Rad) using iTaq Universal SYBR Green master mix (Bio-Rad). The results were analyzed using the comparative Ct method normalized against the housekeeping gene Gapdh. The primer sequences for real-time PCR are as follows:

Rat SLIT1 forward 5′ ATCTAGGTGCTACTCGAGCC 3′,

reverse 5′ TATCTCCAGGTGCTATCCCCA 3′

Rat VWF forward 5′ GCCTCTACCAGTGAGGTTTTGAAG 3′,

reverse 5′ ATCTCATCTCTTCTCTTCTGCTCCAGC 3′

Rat CX3CL1 forward 5′ GAATTCCTGGCGGGTCAGCACCTCGGCATA 3′,

reverse 5′ AAGCTTTTACAGGGCAGCGGTCTGGTGGT 3′

Rat TGFβ1 forward 5′ TCTCGACTCCACACAGT 3′,

reverse 5′ GCCGGGTCATTAGCTATATT 3′

Rat CNTFR forward 5′ TGGTGGTAACGAGATGGCTG 3′,

reverse 5′ GCCCAGACGCTCATACTGAA 3′

Rat RALA forward 5′ GATACAGCAGGGCAGGAAGA 3′,

reverse 5′ GTTCCCTGAAGTCCGCTGTA 3′

Rat IDI1 forward 5′ AGTCGCCAACACCATCTCTT 3′,

reverse 5′ TGCCAATCTAGCGTAGTCCT 3′

Rat SMC4 forward 5′ TGAATAGTATCCCTCCACCCC 3′,

reverse 5′ AGGTCCCAGAATTTTCTCTCCA 3′

Rat TNFα forward 5′ CCCAGACCCTCACACTCAGAT 3′,

reverse 5′ GTCCAAGAGAAGTTCCCTGTT 3′

Rat IL-6 forward 5′ GGGACTGATGTTGTTGACAG 3′,

reverse 5′ GGACCTCAAACACTTCTTGT 3′

Rat GAPDH forward 5′ ACAGCAACTCCCATTCTTCCA 3′,

reverse 5′ TCCAGGGTTTCTTACTCCTTGG 3′

Immunofluorescence staining

Thoracic spinal cord sections were fixed in 4% paraformaldehyde, then immersed in 20% sucrose, mounted with OCT compound, and sectioned at 4-6 μm. Sections were stained with the primary antibodies against substance P (Mouse Anti-SP, 1:1000, Abcam; ab14184), TRPV1 (Rabbit Anti-TRPV1, 1:200, Alomone; ACC-030), Cx3Cl1 (Rabbit Anti-Cx3Cl1, 1:250, ThermoFisher; 14-798681), microglia (Rabbit Anti-IBA1, 1:500, Fujifilm; 01919741), astrocyte (Goat Anti-GFAP, 1:100, Abcam; ab53554), neurons (Mouse Anti-NeuN, 1:500, SigmaAldrich; MAB377), Neuropeptide Y (Rabbit Anti-NPY, 1:200, Proteintech; 128331AP) and cleaved Caspase-3 (Rabbit Anti-Asp175, 1:200, Cell Signaling; 9661). The sections were mounted using Fluoromount G with DAPI (Invitrogen # 00-4959-52). Images were acquired with a confocal microscope (Nikon).

Terminal deoxynucleotidyl transferase dUTP nick end labeling (TUNEL)

TUNEL staining was performed to assess for apoptosis in the thoracic spinal cords of MCT- and SuHx-induced PH rats. Spinal cord sections were subjected to staining with the TUNEL Assay Kit-BrdU-Red (Abcam ab66110) following the manufacturer's manual. The percentage of $TUNEL^+$ cells (integrated optical density) was calculated.

Plasma norepinephrine

Blood samples were collected from MCT- and SuHx-induced PH rats by cardiac puncture into a heparinized blood collection tube (BD Vacutainer, Franklin Lakes, NJ), and centrifuged immediately at 3000g for 10 min at 4°C. Sodium metabisulfite at a final concentration of 4 mmol/L, was added to the plasma to prevent catecholamine

degradation. The enzyme immunoassay for the quantification of plasma norepinephrine levels were carried out in duplicate for each sample using a commercially available kit (Norepinephrine ELISA Kit, abnova, KA1877) following the manufacturer's protocol.

Statistical Analysis

One-way ANOVA tests were used to compare between groups using GraphPad Prism. When significant differences were detected, individual mean values were compared by post-hoc tests that allowed for multiple comparisons. Analyses were run using GraphPad Prism. $P<0.05$ was considered statistically significant. Values are expressed as mean±SD. For RNAseq, differential expression analysis was conducted using the R-program DeSeq2 correcting for multiple hypothesis testing using the Benjamini Hochberg method.

Supplementary Results

Development of Severe PH and RVF in MCT and SuHx Rats

Severe PH and RVF were confirmed using serial transthoracic echocardiography and terminal right heart catheterization in rats treated with MCT or SuHx compared to PBS-treated control rats (Figure S1). Both MCT and SuHx rats developed significant PH as evidenced by increased RV systolic pressure (RVSP) (MCT=94±14; SuHx=93±18, vs. control=37±2mmHg; $p<0.0001$ MCT vs. control, $p<0.0001$ SuHx vs. control) (Figure S1B). Additionally, decreased pulmonary artery acceleration time (PAT) (MCT=19±3; SuHx=18±3 vs. control=32±5ms; $p<0.0001$ MCT vs. control, $p<0.0001$ SuHx vs. control) and pulmonary artery acceleration time/pulmonary ejection time (PAT/PET) (MCT=0.24±0.04; SuHx=0.23±0.03 vs. control=0.41±0.04mmHg; $p<0.0001$ MCT vs. control, $p<0.0001$ SuHx vs. control) ratio also demonstrated severity of PH (Figure S1C, D,J). RV dysfunction was demonstrated by increased RV internal diameter at end-diastole ($RVID_d$) (MCT=3.5±1.04; SuHx=2.9±0.77 vs. control=1.9±0.66mm; $p=0.002$ MCT vs. control, $p=0.032$ SuHx vs. control) and decreased RV fractional area change (RVFAC) (MCT=13±5.35; SuHx=17±3.59 vs. control=40±14.1%; $p=0.0007$ MCT vs. control, $p=0.003$ SuHx vs. control) in MCT and SuHx rats (Figure S1E, F,J). MCT and SuHx rats also demonstrated an increase in Fulton index of RV hypertrophy (MCT=0.8±0.1; SuHx=0.6±0.1 vs. control=0.3±0.01; $p<0.0001$ MCT vs. control, $p=0.001$ SuHx vs. control) (Figure S1G). No significant differences were observed between SuHx- and MCT-treated groups in all the parameters. Left ventricular ejection fraction (LVEF) and left ventricular systolic pressure (LVSP) were preserved between control, MCT and SuHx groups (Figure S1H, I).

Supplementary Figure Legends

Figure S1. Experimental models of severe PH and RV failure in rats. (**A**) Experimental Protocol. (**B**) RV systolic pressure (RVSP, mmHg), (**C**) Pulmonary artery acceleration time (PAT, mS), (**D**) Pulmonary artery acceleration time/Pulmonary ejection time (PAT/PET) ratio, (**E**) RV internal diameter at end diastole ($RVID_d$, mm), (**F**) RV fractional area change (RVFAC, %), (**G**) Fulton index of RV hypertrophy [RV/(LV+IVS)], (**H**) Left ventricular ejection fraction (LVEF, %) and (**I**) LV systolic pressure (LVSP, mmHg) in control, MCT and SuHx groups. (**J**) From top to bottom: Images obtained from rat heart echocardiography in B-mode and pulsed-wave doppler mode from control, MCT and SuHx groups. N=4-8 per group. *p<0.05, **p<0.01, ***p<0.001, ****p<0.0001.

Figure S2. Volcano plot of log fold change vs. mean expression for all genes from thoracic spinal cords for comparing MCT vs. Control groups. Differentially expressed genes with FDR <0.05 are represented as red dots.

Figure S3. Volcano plot of log fold change vs. mean expression for all genes from thoracic spinal cords for comparing SuHx vs. Control groups. Differentially expressed genes with FDR <0.05 are represented as red dots.

Figure S4. Bar plot showing normalized enrichment scores (NES) for Hallmark pathways derived from Gene Set Enrichment Analysis (GSEA). For GSEA, differentially expressed genes between MCT vs. Control were ranked by the Wald statistic derived from DESeq2. Bars in blue and red represent statistically significant (FDR<0.05) pathways up- and downregulated, respectively.

Figure S5. Bar plot showing normalized enrichment scores (NES) for Hallmark pathways derived from Gene Set Enrichment Analysis (GSEA). For GSEA, differentially expressed genes between SuHx vs. Control were ranked by the Wald statistic derived from DESeq2. Bars in blue and red represent statistically significant (FDR<0.05) pathways up- and downregulated, respectively.

Figure S6. Time dependent increase of PH, TSC neuroinflammation, apoptosis and associated sympathoexcitation in MCT-induced PH rats. (**A**) Experimental Protocol. (**B**) Right ventricular systolic pressure (RVSP) at day-0 (Control), -7 and -14 after MCT injection. N=6 per group, ****p<0.0001. (**C**) Fulton index at day-0 (Control), -7 and -14 after MCT injection. N=3 per group, *p<0.05, **p<0.01. (**D**) B-Mode echo and PA Doppler at day-0 (Control), -7 and -14 after MCT injection. (**E**) Representative images of immunofluorescence staining with microglial marker anti-Iba1 (Red), astrocytic marker anti-GFAP (Green) and DNA marker DAPI (Blue) in the TSC of rats at day-0 (Control), -7 and -14 after MCT injection. N=3 per group. (**F**) Representative images of immunofluorescence staining with neuronal marker NeuN (Red), Cx3Cl1 (Green) and DAPI (Blue) in the TSC of rats at day-0 (Control), -7 and -14 after MCT injection. N=3 per group. (**G**) Normalized qRT-PCR data of pro-apoptotic gene TGFβ1expression in the TSC from rats at day-0 (Control), -7 and -14 after MCT injection. N=3 per group. (**H**) Quantification of number of microglia/HPF in the TSC from rats at day-0 (Control), -7 and

-14 after MCT injection. (**I**) Percent activated microglia/HPF in the TSC from rats at day-0 (Control), -7 and -14 after MCT injection. N=3 per group. ***p<0.001. (**J**) normalized qRT-PCR data of pro-inflammatory gene Cx3Cl1 expression in the TSC from rats at day-0 (Control), -7 and -14 after MCT injection. N=3 per group. **p<0.01. (**K**) Plasma norepinephrine level measured by ELISA from rats at day-0 (Control), -7 and -14 after MCT injection. N=6 per group.

Figure S7. Increased NPY in the ventral horn of TSC and circulating catecholamines as markers of sympathoexcitation in MCT- and SuHx-induced PH. (**A**) Representative images of immunofluorescence staining with anti-NPY (Red), anti-NeuN (Green), and DAPI (DNA; blue) from ventral horn gray matter. Lower panel shows enlarged view of NPY and NeuN colocalization (Yellow) in control compared with MCT (day 28) and SuHx (day 35). N=3 per group. (**B**) Plasma norepinephrine levels measured by ELISA are significantly increased in MCT (day 28) and SuHx (day 35) rats compared to controls. N=5-6 per group. ***p<0.001, ****p<0.0001.

Figure S8. RNA-Seq based pathway enrichment analysis from TSC, right ventricles and lungs of MCT and SuHx rats. (**A**) Venn diagram showing significantly up-regulated pathways (based on FDR<0.05) and their overlap in thoracic spinal cords, right ventricles and lungs of MCT and SuHx groups respectively. (**B**) Venn diagram showing common significantly up-regulated pathways (based on FDR<0.05) in TSC, RV and lung highlighting proinflammatory signature in MCT- and SuHx-induced PH.

Figure S9. Increased neuronal apoptosis in the TSC of MCT and SuHx rats. Representative images of immunofluorescence staining with DAPI (DNA; blue), anti-NeuN (Neuron; Green), anti-Cleaved Caspase-3 (CC3; Red), CC3 and DAPI colocalization, NeuN and CC3 colocalization (Yellow) merged images from the TSC of control, MCT and SuHx rats. N=3 per group.

Supplementary References

1. Korotkevich G, Sukhov V, Sergushichev A. Fast gene set enrichment analysis. bioRxiv 2019;060012.doi:10.1101/060012.
2. Liberzon A, Birger C, Thorvaldsdóttir H, Ghandi M, Mesirov JP, Tamayo P. The Molecular Signatures Database (MSigDB) hallmark gene set collection. Cell Syst 2015;1:417–425.
3. Subramanian A, Tamayo P, Mootha VK, Mukherjee S, Ebert BL, Gillette MA, Paulovich A, Pomeroy SL, Golub TR, Lander ES, Mesirov JP. Gene set enrichment analysis: a knowledge-based approach for interpreting genome-wide expression profiles. Proc Natl Acad Sci USA 2005;102:15545–15550.

Table S1: Leading edge upregulated genes from MCT vs. Control

Hedgehog signaling	log2FC	padj	Hypoxia	log2FC	padj	Apical junction	log2FC	padj	Myogenesis	log2FC	padj	Epithelial mesenchymal transition	log2FC	padj	KRAS signaling dn	log2FC	padj
SLIT1	1.52923316	0.00132072	SERPINE1	2.15703066	0.00327275	VWF	1.93667602	3.81E-07	NOS1	2.91473019	0.00040949	SERPINE1	2.15703066	0.00327275	NOS1	2.91473019	0.00040949
L1CAM	1.2196331	0.00047839	MAFF	1.1804272	0.02459397	ATP1A3	1.47410359	3.37E-06	CACNA1H	1.30269704	0.00187157	COL4A1	1.21253977	0.00025107	SGK1	2.02187581	0.01781026
CNTFR	0.86338726	0.00040688	CTGF	1.12729245	0.00067825	ZYX	1.10264733	5.44E-08	CDKN1A	1.02703503	0.04111099	CTGF	1.12729245	0.00067825	CELSR2	1.92733061	0.00127072
ACHE	0.84116685	0.00012776	CDKN1A	1.02703503	0.04111099	NLGN2	1.01713745	0.00117823	TGFB1	0.95957948	0.01221739	ECM1	1.07790511	0.00758918	TCF7L1	1.29676197	0.00398718
NKX6-1	0.75475976	0.01954071	PFKL	1.00351614	1.55E-07	COL16A1	0.9830112	0.0150533	ACHE	0.84116685	0.00012776	FN1	1.00943264	3.00E-05	SLC5A5	1.2026906	0.00402044
VEGFA	0.64377283	0.02339733	NFIL3	0.84625767	0.0314438	JUP	0.8510631	0.01100947	MEF2D	0.82017115	0.0116954	COL16A1	0.9830112	0.0150533	SYNPO	1.15896479	0.00011156
TLE3	0.60021556	1.27E-06	IRS2	0.78999334	0.01191473	PKD1	0.83950447	0.00702429	GAA	0.74347084	0.00122352	SLIT3	0.97152188	0.00684493	EDN1	1.13918079	2.54E-06
CRMP1	0.49279734	0.03708276	ZFP36	0.77347349	0.00413902	NRXN2	0.82213913	0.00401279	GNAO1	0.70545644	0.00758918	TGFB1	0.95957948	0.01221739	ABCG4	0.93616392	0.00612042
RTN1	0.41531716	0.02179859	FOXO3	0.77076389	7.34E-05	FLNC	0.81853833	0.01739358	LPIN1	0.66252503	7.19E-06	LRP1	0.88346029	0.00301657	CLSTN3	0.90075433	0.00010213
LDB1	0.24365635	0.04444929	SLC2A1	0.74979411	2.65E-06	CX3CL1	0.80803224	0.00927777	SPTAN1	0.66097616	0.00711834	BGN	0.71395918	0.04776776	CNTFR	0.86338726	0.00040688

Table S2: Leading edge downregulated genes from MCT vs. Control

Oxidative phosphorylation	log2FC	padj	MYC targets v1	log2FC	padj	E2F targets	log2FC	padj	Fatty acid metabolism	log2FC	padj	G2M checkpoint	log2FC	padj	Protein secretion	log2FC	padj
ATP5I	-0.4602775	0.03014973	HSPE1	-0.4663213	0.0344881	HMMR	-0.5156615	0.00726704	IDI1	-0.9945439	2.85E-08	HMMR	-0.5156615	0.00726704	VAMP3	-0.4824885	0.00081044
HSD17B10	-0.4101781	0.02629044	SNRPB2	-0.4023445	0.0434563	PRIM2	-0.5146526	0.01640269	HMGCS1	-0.7918761	0.0395009	PRIM2	-0.5146526	0.01640269	RAB9A	-0.4238423	0.00604386
NDUFB5	-0.4096467	0.03641204	EIF1AX	-0.3749151	0.00840991	SMC4	-0.5053989	0.00069059	ALDH1A1	-0.525869	0.03224216	SMC4	-0.5053989	0.00069059	ARFIP1	-0.3679903	0.02110056
IDH1	-0.4018254	2.26E-05	ABCE1	-0.3419424	0.00023078	PLK4	-0.4664285	0.00996213	MCEE	-0.4607909	0.01928823	PLK4	-0.4664285	0.00996213	TMED2	-0.3091218	0.00594054
CYB5A	-0.3894884	0.01111554	EIF3J	-0.3413659	0.00404205	NASP	-0.3941683	0.00620641	HSD17B10	-0.4101781	0.02629044	KATNA1	-0.3945287	0.01961316	PPT1	-0.2441644	0.01115309
SDHC	-0.3624935	0.00643443	YWHAQ	-0.3406791	0.00277792	CBX5	-0.309343	0.04920589	IDH1	-0.4018254	2.26E-05	NASP	-0.3941683	0.00620641	GLA	-0.2226622	0.01178948
MRPL35	-0.3476328	0.03243418	EIF4A1	-0.337197	0.01133372	IPO7	-0.2848156	0.03661852	RDH11	-0.4004075	0.04287412	HIF1A	-0.2981458	0.0020636	RER1	-0.2076079	0.04832511
MRPS22	-0.3048557	0.0230967	HNRNPA1	-0.264461	0.02074197	EED	-0.2829055	0.02394236	HIBCH	-0.3830768	0.00297677	DTYMK	-0.2337329	0.04763575			
PRDX3	-0.2616599	0.01824858	CLNS1A	-0.2642205	0.02434174	AK2	-0.2786334	0.03587913	SDHC	-0.3624935	0.00643443	CTCF	-0.1979872	0.02459704			
HADHB	-0.2521579	0.0004723	PRDX3	-0.2616599	0.01824858	CSE1L	-0.2742685	0.00081044	ECI2	-0.3311596	0.03449003						

Table S3: Leading edge upregulated genes from SuHx vs. Control

Myogenesis	log2FC	padj	Apical junction	log2FC	padj	Hedgehog signaling	log2FC	padj	TNFa signaling via NFkB	log2FC	padj	Epithelial mesenchymal transition	log2FC	padj	Estrogen response early	log2FC	padj
NOS1	2.99711754	0.00011287	MYH9	2.23323215	0.05273871	SLIT1	1.89100726	1.99E-05	PER1	1.64049986	6.75E-05	TGFB1	1.27447756	0.00023292	CELSR2	2.20487632	7.69E-05
MYH9	2.23323215	0.05273871	ATP1A3	1.64037253	9.35E-08	L1CAM	1.4697053	6.94E-06	BCL3	1.577725	0.01898447	ECM1	1.24368912	0.0007332	NCOR2	1.79553703	2.00E-05
CACNA1H	1.56660571	5.31E-05	VWF	1.54761153	3.89E-05	ACHE	0.91605159	9.63E-06	KDM6B	1.44012204	0.00190701	SLIT3	1.12042022	0.00062203	CBFA2T3	1.38491412	0.00198345
TGFB1	1.27447756	0.00023292	NLGN2	1.20663041	3.53E-05	CNTFR	0.90803833	7.56E-05	NR4A1	1.34410983	0.00113308	COL4A1	1.1165481	0.00034093	WFS1	1.37086532	0.00053893
SOD3	1.24042158	0.00013149	CX3CL1	1.17070771	3.24E-05	NRP2	0.7289368	0.0379429	KLF2	1.18702462	1.84E-07	COL5A1	1.08843298	0.01862121	TJP3	1.30989669	0.02753758
NAV2	1.19070543	0.00736234	NRXN2	1.12139226	1.99E-05	NKX6-1	0.64121584	0.03201497	ZFP36	1.14086035	3.96E-06	CYR61	1.05610837	0.00128525	FLNB	1.21169322	0.00879893
MEF2D	0.97735456	0.00092609	ZYX	1.11408757	2.27E-08	TLE3	0.63564196	1.19E-07	CEBPB	1.06326416	0.0023259	COL16A1	1.02293558	0.00558921	NAV2	1.19070543	0.00736234
AGRN	0.95444814	0.00594105	COL16A1	1.02293558	0.00558921	RTN1	0.61294823	0.00015805	BTG2	1.06097519	0.00622523	LRP1	1.01943875	0.0002044	IGF1R	0.91300154	0.00293567
GAA	0.94641479	9.85E-06	JUP	1.00386351	0.00096895	CRMP1	0.58951571	0.00526393	EGR1	1.05773067	0.01987758	NOTCH2	0.94910812	0.00047049	FASN	0.85202853	0.02557508
MYOM2	0.93847503	0.01610441	PKD1	0.95409753	0.0008152	ETS2	0.39151693	0.02274943	CYR61	1.05610837	0.00128525	BGN	0.94102143	0.00317483	RET	0.81686885	1.73E-09

Table S4: Leading edge downregulated genes from SuHx vs. Control

MYC targets v1	log2FC	padj	Oxidative phosphorylation	log2FC	padj	Protein secretion	log2FC	padj	E2F targets	log2FC	padj	Fatty acid metabolism	log2FC	padj	mTORC1 signaling	log2FC	padj
MAD2L1	-0.6506953	0.01238654	CYCS	-0.6540507	0.01289529	STX7	-0.6860614	0.04223023	PAICS	-0.7376966	6.22E-06	CIDEA	-1.6971151	0.00011225	ELOVL6	-1.4139301	0.01643881
PSMC6	-0.6283155	0.00660682	ETFA	-0.6368364	0.00190588	YIPF6	-0.681641	0.00132626	SMC4	-0.691634	6.67E-07	IDI1	-1.0501473	1.73E-09	IDI1	-1.0501473	1.73E-09
SNRPB2	-0.6065325	0.00054773	TIMM8B	-0.6331286	0.03408694	CAV2	-0.6310332	0.00049914	MAD2L1	-0.6506953	0.01238654	OSTC	-0.5806135	0.00548695	PRDX1	-0.6667162	3.67E-05
EIF2S2	-0.6017194	0.00059868	COX6C	-0.5648643	0.03220819	VAMP7	-0.6033581	0.00014836	PLK4	-0.6486813	8.26E-05	HSD17B10	-0.5639058	0.00061283	TM7SF2	-0.6529173	0.01212614
PRDX4	-0.5738238	0.00119421	HSD17B10	-0.5639058	0.00061283	VAMP3	-0.5645947	2.78E-05	RPA3	-0.5991998	0.00501784	ALDH1A1	-0.5373104	0.01581011	PSMC6	-0.6283155	0.00660682
SNRPD1	-0.5626125	0.00843077	ATP5L	-0.5582338	0.04036535	SNAP23	-0.5637627	0.00222131	HMMR	-0.5895495	0.0007792	IDH1	-0.4898324	4.67E-08	TCEA1	-0.618892	0.00219411
RPL22	-0.5624908	0.01668785	COX7C	-0.5560833	0.04235892	BET1	-0.5588287	0.00333788	PRDX4	-0.5738238	0.00119421	HIBCH	-0.4882273	3.89E-05	PSMA3	-0.6038286	0.00175107
PPIA	-0.5316288	0.01970254	NDUFV2	-0.5516004	0.04313666	ARFIP1	-0.5546454	0.00011181	GINS4	-0.5442734	0.00738578	PTS	-0.4749547	0.00506911	EIF2S2	-0.6017194	0.00059868
NPM1	-0.5314841	0.02614638	CYB5A	-0.5515572	7.56E-05	RAB5A	-0.5544714	0.00085748	TIPIN	-0.5264054	0.02693264	DECR1	-0.4701517	0.00462211	CD9	-0.5453986	3.81E-05
HDDC2	-0.5256748	0.00680919	ATP6V1G1	-0.5435872	0.00582496	TPD52	-0.5037851	0.00090371	PRIM2	-0.5088931	0.00935769	DLD	-0.4439073	0.01595298	PPIA	-0.5316288	0.01970254

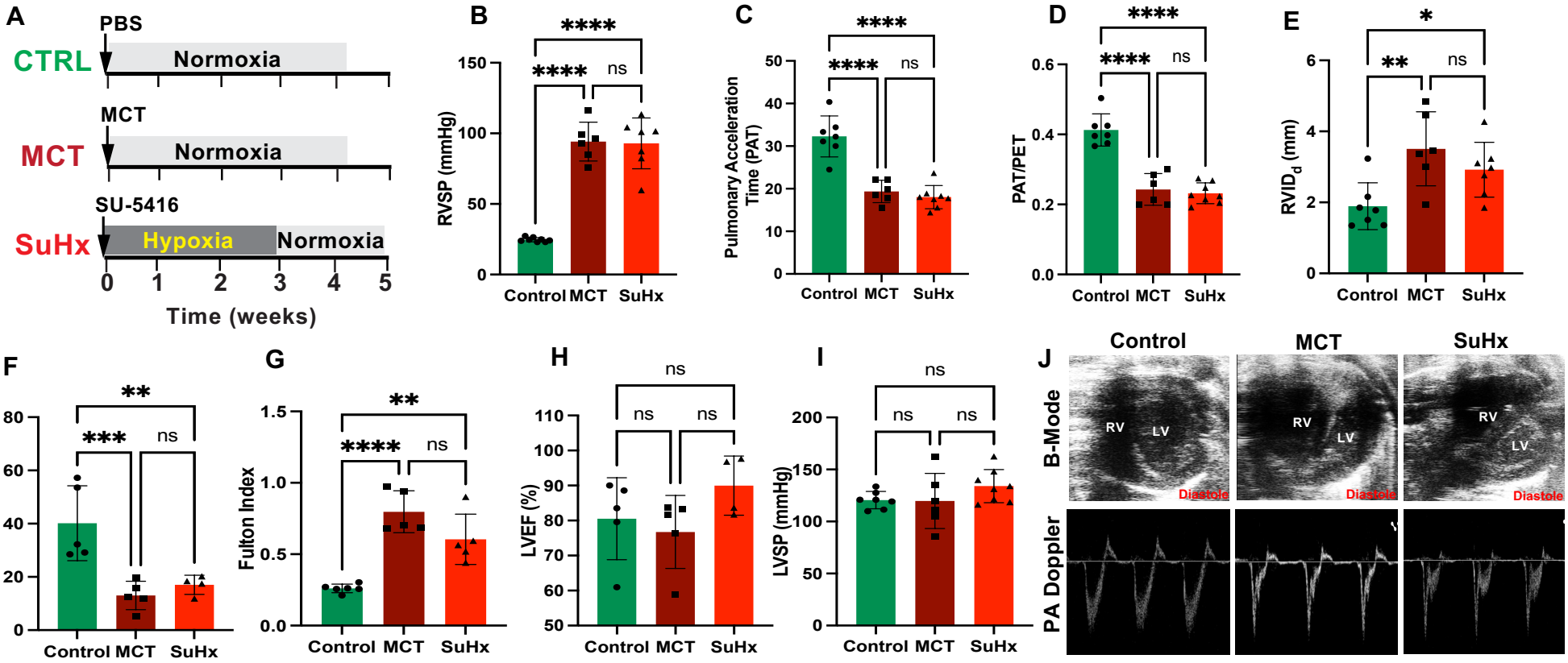

Fig. S1, Razee *et al.*

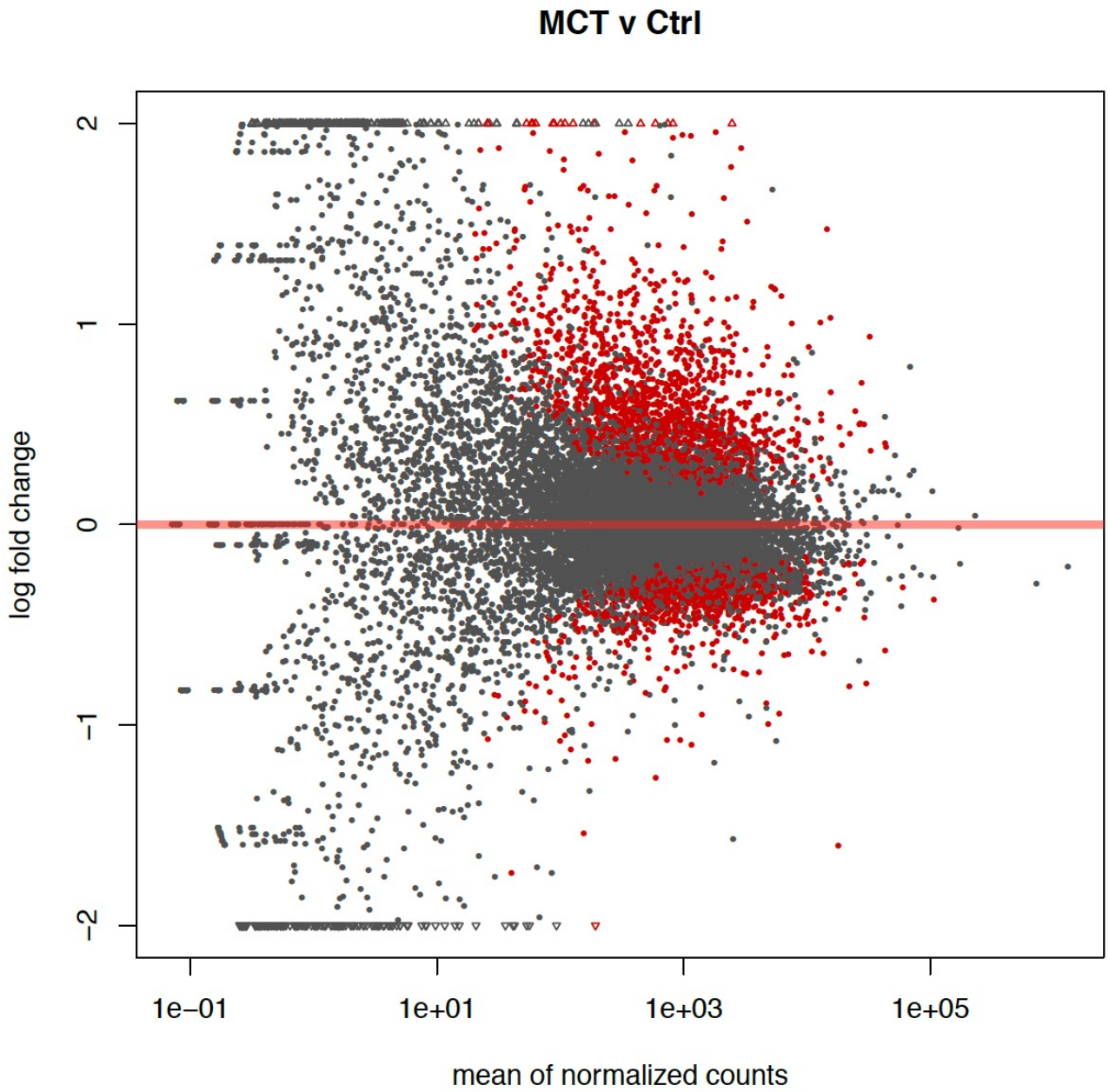

Fig. S2, Razee *et al.*

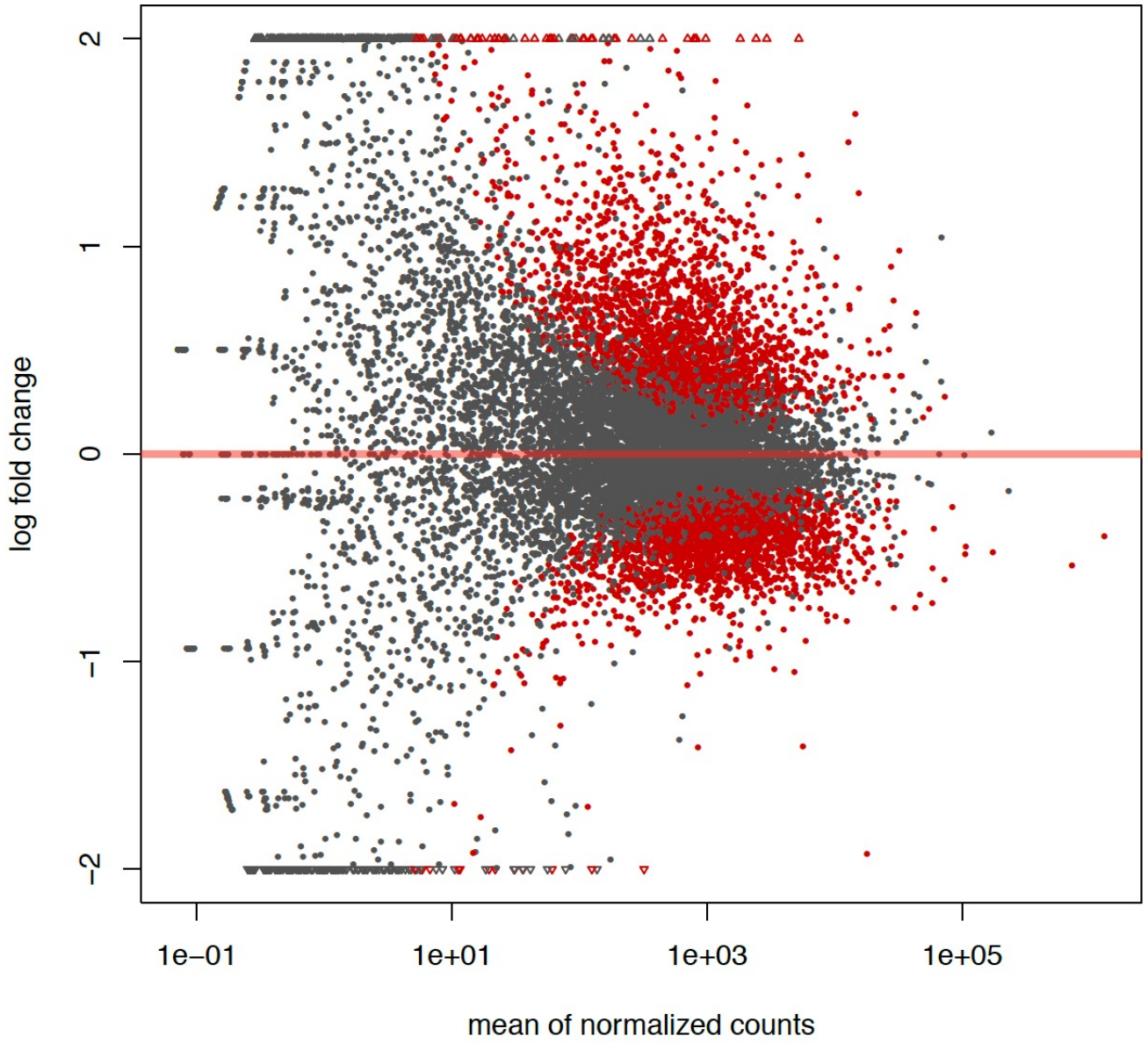

Fig. S3, Razee *et al.*

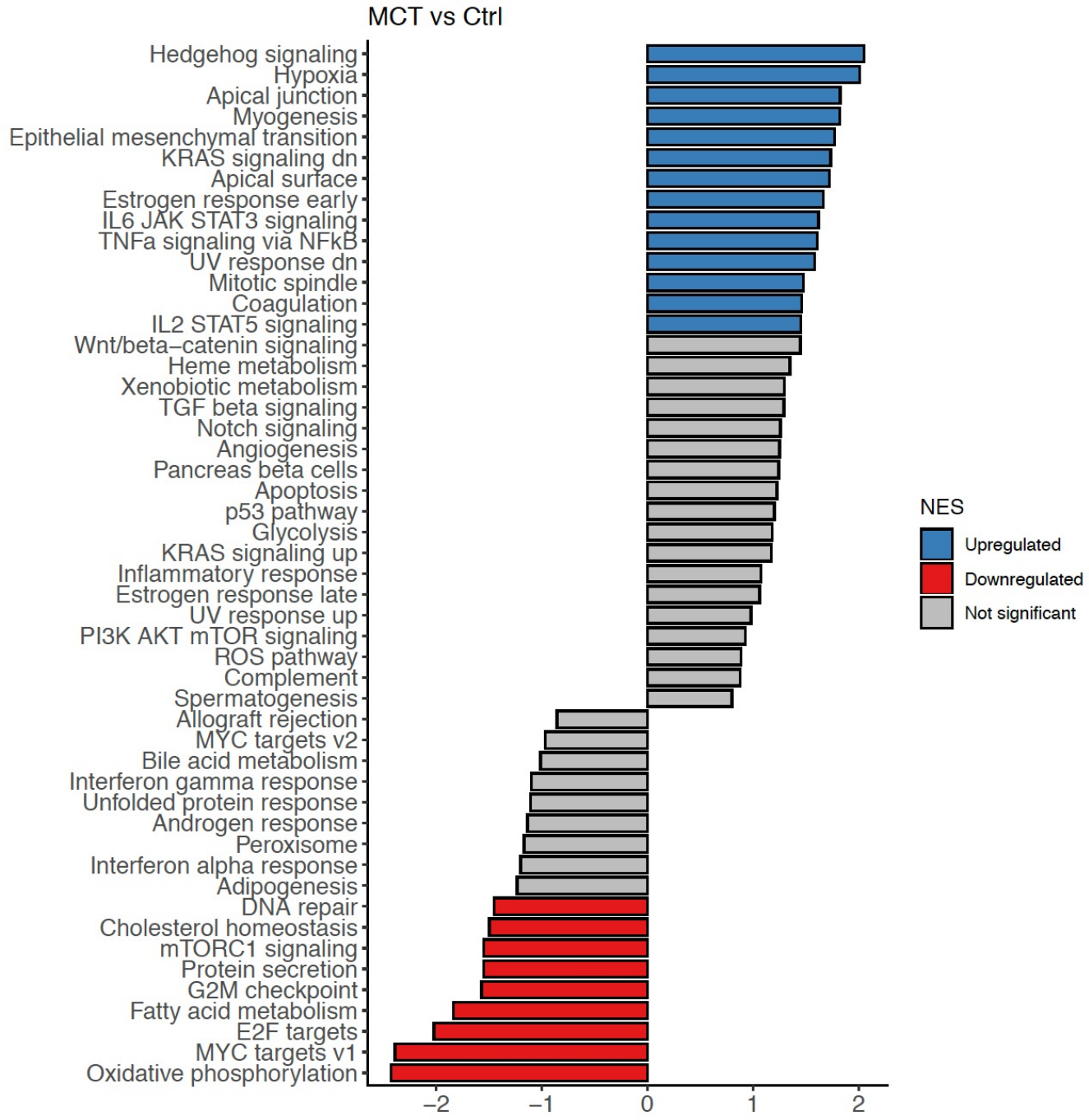

Fig. S4, Razee *et al.*

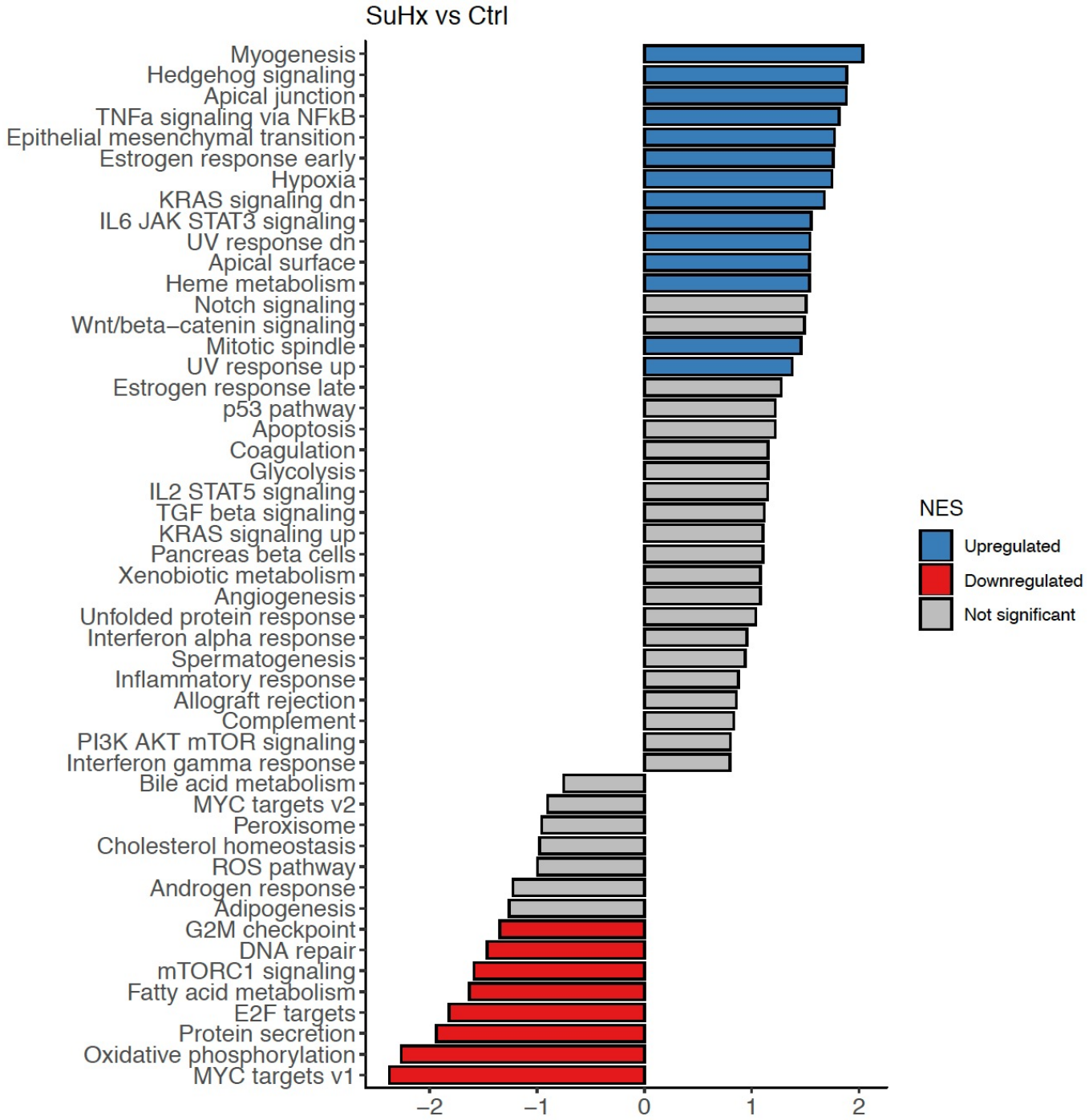

Fig. S5, Razee *et al.*

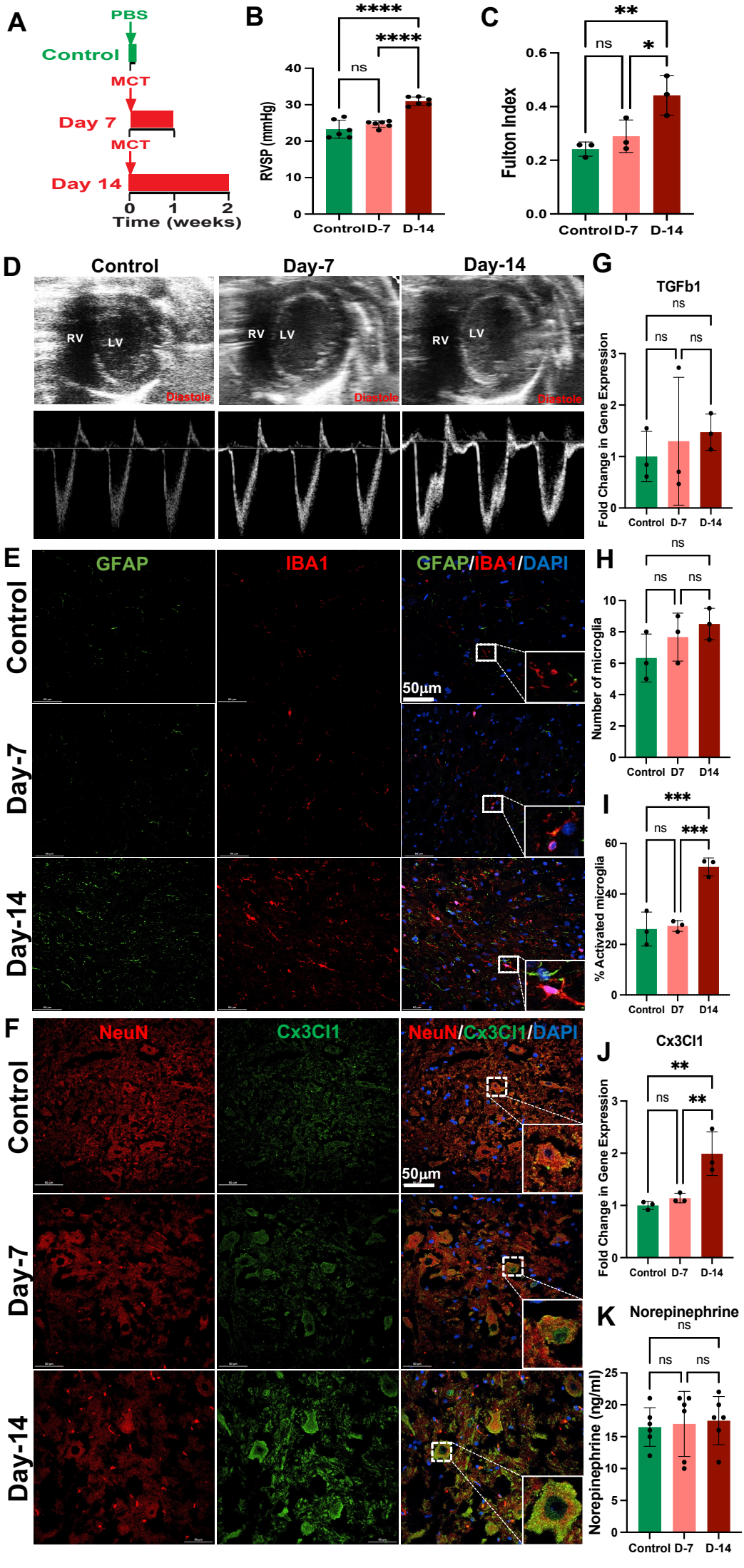

Figure S6, Razee *et al.*

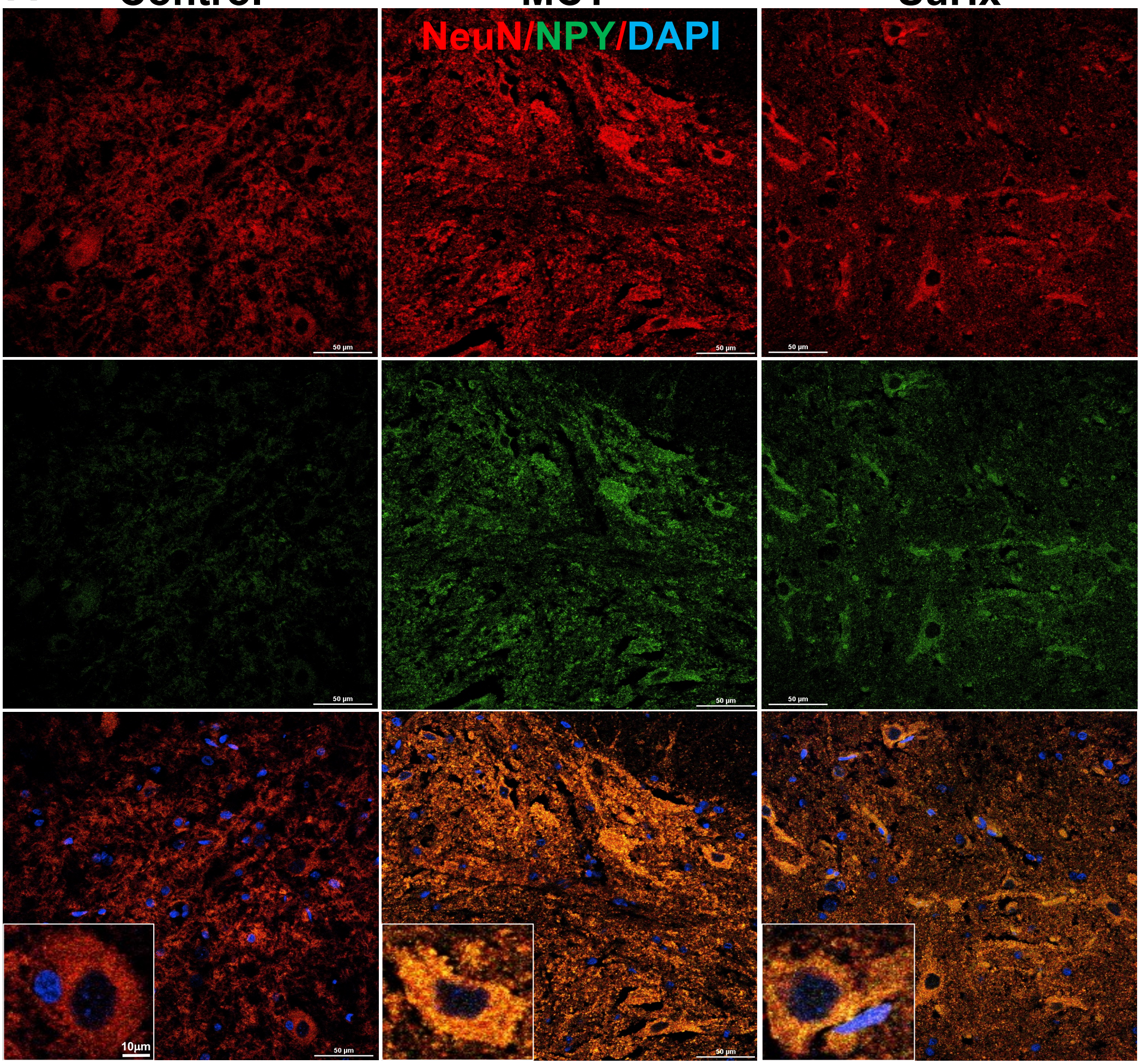

Fig. S7, Razee et al

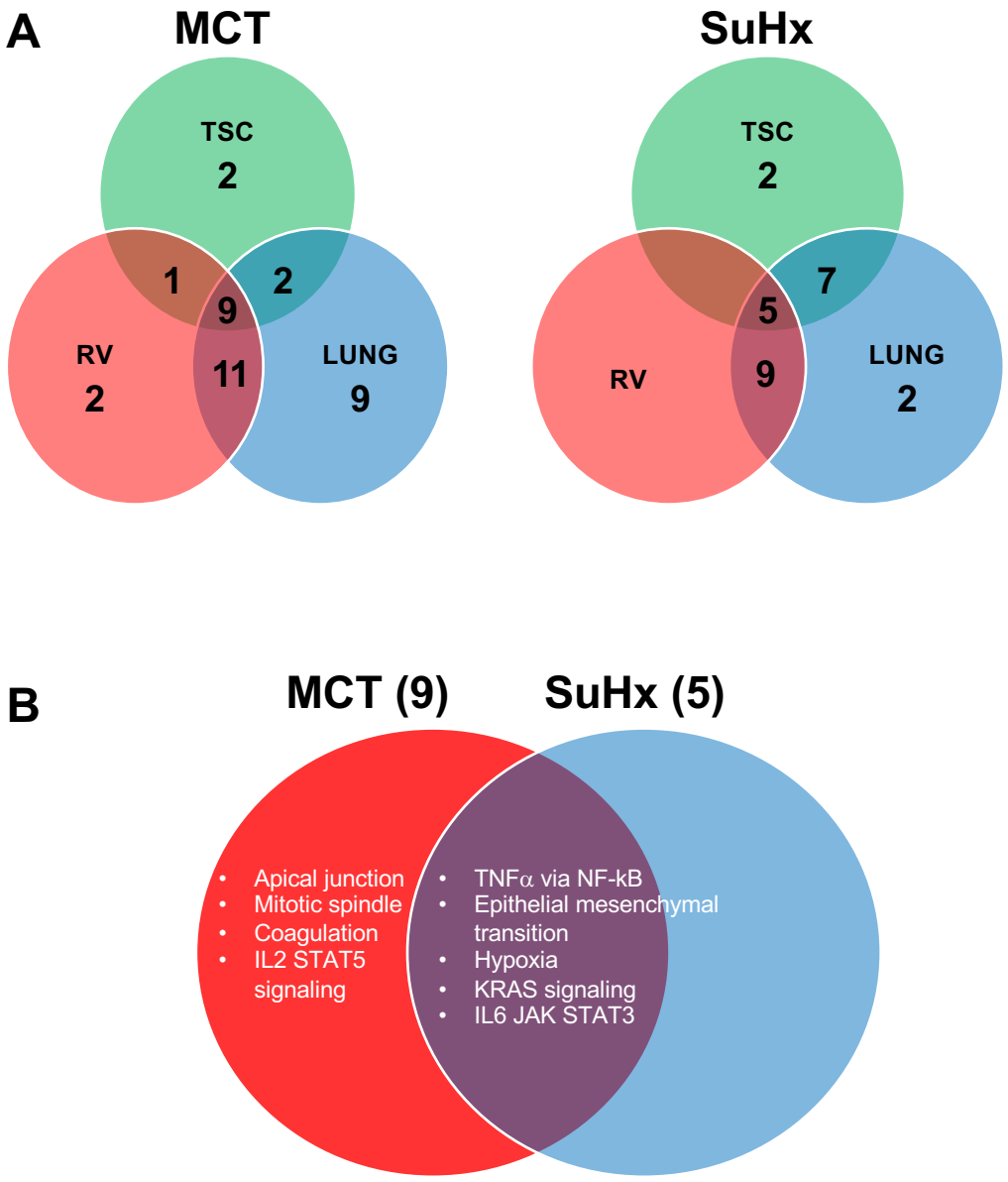

Fig. S8, Razee et al

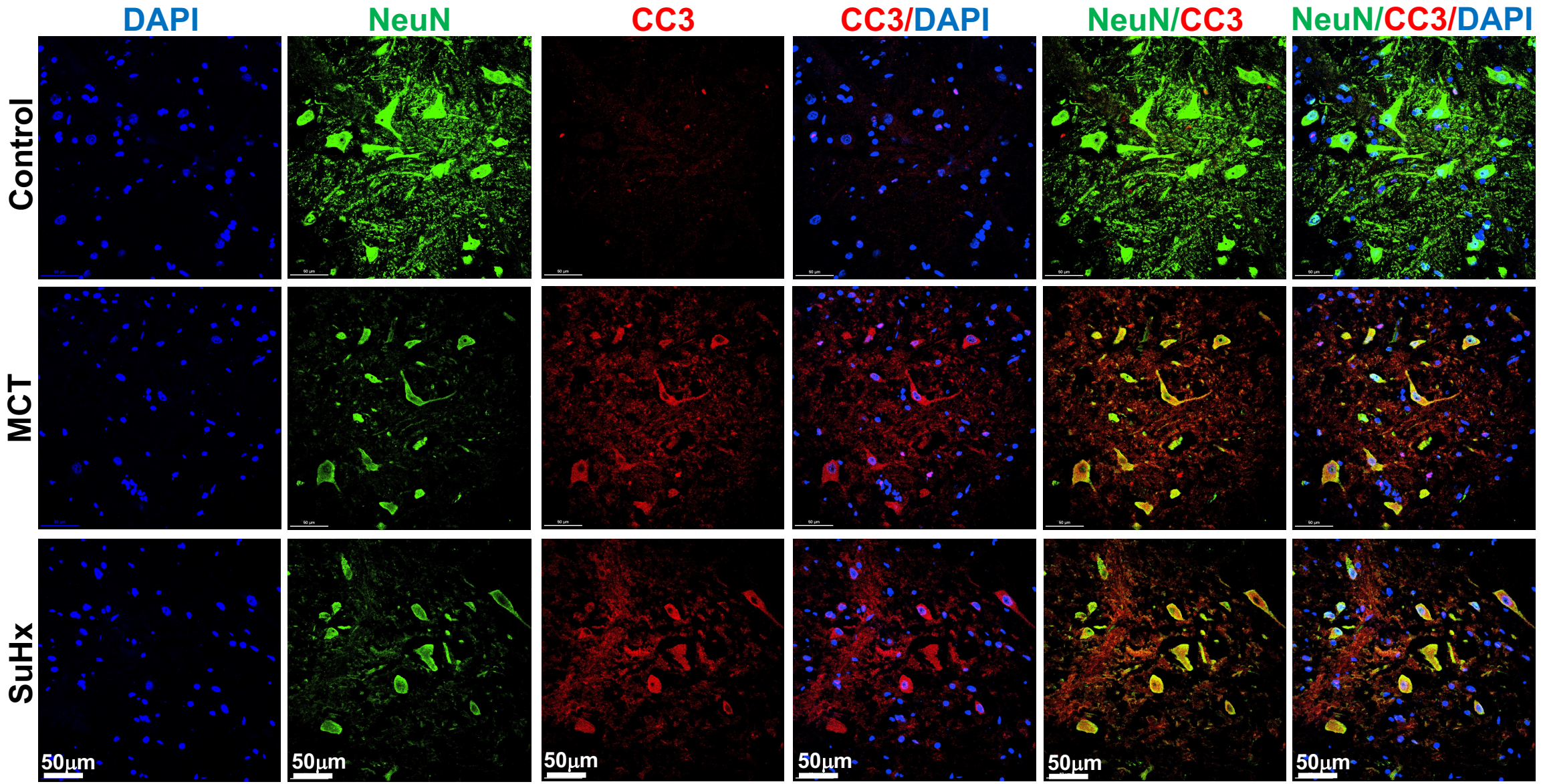

Fig. S9, Razee *et al.*